

# Random Matrix Theory, Atmospheric Turbulence, and Free-Space Optical Communications

Manishika Agaskar

May 10, 2016

## Introduction

In the past few years, there has been growing interest in applying random matrix theory results to communications and signal processing. This report discusses that work in the specific context of free-space optical communications. Free-space optical (FSO) communication is an attractive medium for high data-rate terrestrial communications; in addition to enabling potentially Gbps communications, FSO systems are less expensive to deploy than fiber, relatively portable, and do not have the licensing requirements of radio frequency (RF) communications. For point-to-point, line-of-sight communications requirements, FSO links are an obvious solution.

A major disadvantage of these terrestrial links is the limiting impact of atmospheric turbulence, which induces microscale fluctuations of temperature and index of refraction, causing phase distortion of the transmitted optical waveform. The effects of turbulence can be mitigated by increasing the transmit power, increasing the temporal diversity of the transmitted signal (e.g via bit interleaving), or increasing the spatial diversity of the transmitted signal (e.g via a sparse aperture array design). It is this last method of turbulence mitigation via spatial diversity that is discussed in this report.

The theoretical results in this report are proved in the 2009 paper “Optical Communication Through the Turbulent Atmosphere with Transmitter and Receiver Diversity, Wavefront Control, and Coherent Detection” by Puryear and Chan [1] and in Puryear’s 2011 PhD thesis of the same title [2]. My goal in this project was to understand, summarize, and simulate the results developed in [1] and [2], in order to answer the question: *how does random matrix theory help us understand the performance bounds of a free-space optical communications link in atmospheric turbulence?*

## Channel Setup

To mitigate atmospheric turbulence, we can employ spatial diversity via a sparse aperture system architecture, illustrated in Figure 1. The sparse aperture system as described in [1] is comprised of an array of  $n_{tx}$  apertures in the transmit plane  $\rho$  transmitting a signal to an array of  $n_{rx}$  detectors in the receive plane. The power from a single coherent laser source is divided via an optical power splitter among the  $n_{tx}$  transmitters. This optical power splitter controls the amplitude of the optical wave emitted by each transmitter. The phase of each wave is adjusted by a phase modulator connected to each aperture. The amplitude and phase are assumed constant over each aperture. The receive plane  $\rho'$  contains an array of  $n_{rx}$  coherent detectors. As the light from the transmit plane propagates through space to the receive plane, the scalar waves from each aperture interfere constructively and destructively to produce the Fraunhofer far-field radiation pattern at the receive plane. This received field is detected and processed to generate a output statistic for the transmission. We can model the channel as

$$\vec{y} = \sqrt{\frac{\text{SNR}}{n_{rx}}} \mathbf{H} \vec{x} + \vec{w}$$

The vector  $\vec{x}$  contains the amplitude and phase of the output field at each transmit aperture, and  $\vec{y}$  the amplitude and phase of the received field at each receive aperture.

$\mathbf{H}$  is the channel transfer matrix, with element  $h_{mn}$  representing the diffraction gain of the field from transmit aperture  $m$  to receive aperture  $n$ . SNR is signal-to-noise ratio for a single aperture transmitter to a single aperture receiver with no turbulence, and  $\vec{w}$  is circularly symmetric complex additive white Gaussian noise with unit variance.

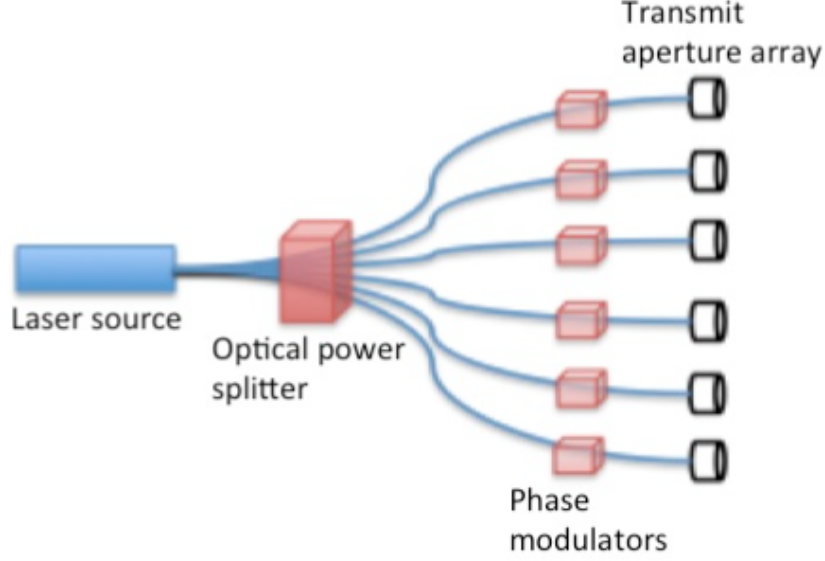


Figure 1: Light from a single laser source is divided by a variable optical power splitter and coupled into an array of apertures, each modulated by an independent phase modulator.

Each element  $h_{mn}$  of the matrix  $\mathbf{H}$  represents the change in phase of the field from transmit aperture  $m$  to receive aperture  $n$ . Then in the noiseless case, the  $n^{\text{th}}$  element of  $\vec{y}$  consists of the sum of the phases of the fields transmitted from each aperture. This sum represents the interference. In the absence of turbulence, the direct path gain from transmitter  $m$  to receiver  $n$  is:

$$h_{mn} = e^{jk \frac{|\rho'_n - \rho_m|^2}{2L}} e^{jkL + j\frac{\pi}{2}}$$

$L$  is the distance between the transmit and receive planes  $\rho$  and  $\rho'$ .  $k$  is the wavenumber,  $2\pi/\lambda$ , where we take  $\lambda = 10^{-6}$ .

As in [2], we use the Rytov approximation to account for the effects of turbulence by multiplying each element of  $\mathbf{H}$  with a turbulence fading factor:

$$e^{\chi(\rho'_n, \rho_m) + j\phi(\rho'_n, \rho_m)}$$

where

$$\chi(\rho'_n, \rho_m) \sim \mathcal{N}(m_\chi, \sigma_\chi^2)$$

$$\phi(\rho'_n, \rho_m) \sim \mathcal{N}(m_\phi, \sigma_\phi^2)$$

This is both an amplitude and phase multiplier. Because energy must be conserved,  $\mathbb{E}[e^{\chi^2} = 1]$ , which means that  $m_\chi = -\sigma_\chi^2$ . Additionally, if  $\sigma_\phi^2 \gg 2\pi$ , then  $\phi(\rho'_n, \rho_m) \sim \text{Unif}[0, 2\pi]$ . This means that:

$$\begin{aligned} h_{mn} &= e^{\chi(\rho'_n, \rho_m) + j\phi(\rho'_n, \rho_m)} e^{jk \frac{|\rho'_n - \rho_m|^2}{2L}} e^{jkL + j\frac{\pi}{2}} \\ &= e^{\chi(\rho'_n, \rho_m) + j\phi(\rho'_n, \rho_m)} \end{aligned}$$

We assume the entries of  $\mathbf{H}$  are independent and identically distributed. If within the transmit and receive planes, the apertures are separated by at least an atmospheric correlation length, then the fading

factor for each path is independent. If the distance between the transmit and receive planes is much greater than distance between apertures, then the lengths of the  $n_{rx} \times n_{tx}$  paths are approximately equal, and thus the fading factor statistics are identical for each path. Additionally, if the bit period is much less than atmospheric correlation time, then we can consider the turbulence statistics to be stationary.

Lastly, we note that we can write the channel transfer matrix as its singular value decomposition and thus calculate the diffraction gain associated with the spatial ‘‘eigenmodes’’ of the matrix.

$$\frac{1}{\sqrt{n_{rx}}} \mathbf{H} = \mathbf{U} \mathbf{\Gamma} \mathbf{V}^\dagger$$

$\vec{u}_i$ , the  $i^{th}$  column of  $\mathbf{U}$ , is the  $i^{th}$  output spatial eigenmode.  $\vec{v}_i$ , the  $i^{th}$  column of  $\mathbf{V}$ , is the  $i^{th}$  input spatial eigenmode.  $\mathbf{\Gamma}$  is the diagonal matrix of singular values  $\gamma$  of  $\mathbf{H}$ , and  $\gamma_i^2$  is the diffraction gain of the  $i^{th}$  spatial eigenmode. To obtain performance bounds for this channel, we now consider the distribution of  $\gamma^2$  as  $n_{tx}, n_{rx} \rightarrow \infty$  while  $\beta = n_{tx}/n_{rx}$  remains fixed.

## Performance Bounds

### Convergence to Marcenko-Pastur Density

The spatial eigenmode diffraction gains, or squared singular values of  $\mathbf{H}/\sqrt{n_{rx}}$ , are equal to the eigenvalues of  $\mathbf{H}\mathbf{H}^\dagger/n_{rx}$ . The nonzero eigenvalues of  $\mathbf{H}\mathbf{H}^\dagger/n_{rx}$  should converge to the Marcenko-Pastur density as  $n_{tx}, n_{rx} \rightarrow \infty$ :

$$f(\gamma^2; \beta) = \frac{\sqrt{\max[0, x - (1 - \sqrt{\beta})^2] \max[0, (1 + \sqrt{\beta})^2 - x]}}{2\pi\gamma^2\beta}$$

We limit our empirical distribution to nonzero squared singular values and do not include the point mass at the origin of the Marcenko-Pastur density.

Figures 2 and 3 compare simulated distributions  $\hat{f}(\gamma^2; \beta)$  with the limiting Marcenko-Pastur density. In all simulations, the distance between the receive and transmit planes was 10 kilometers. The distributions in Figure 2 were computed under a weak turbulence assumption, such that  $\sigma_\chi^2 \approx 0.0228$ . Figure 3 shows the distribution of diffraction gains under a strong turbulence assumption, where  $\sigma_\chi^2 = 0.5$ .

We expect the convergence under strong turbulence to be slower than that for weak turbulence because the rate of decrease for the higher moments of the matrix elements will be slower due to the larger variance. In Figure 2, for  $n_{tx} = 100$ , the theoretical density is very close to the empirical distribution regardless of  $\beta$ . In Figure 3, under strong turbulence, we see that the  $\beta = 0.1$  case (which has  $n_{rx} = 1000$ ) is visibly better than  $\beta = 1$  or  $0.5$  with fewer receive apertures. In both figures, we can see the convergence of the empirical distribution from left to right (as  $n_{rx}$  increases) and from top to bottom (as  $n_{tx}$  increases).

We also note that the largest singular value is greater for systems with larger  $\beta$ . This means that we can achieve a greater diffraction gain by optimizing the wavefront when we have more transmit apertures with respect to a fixed number of receive apertures.

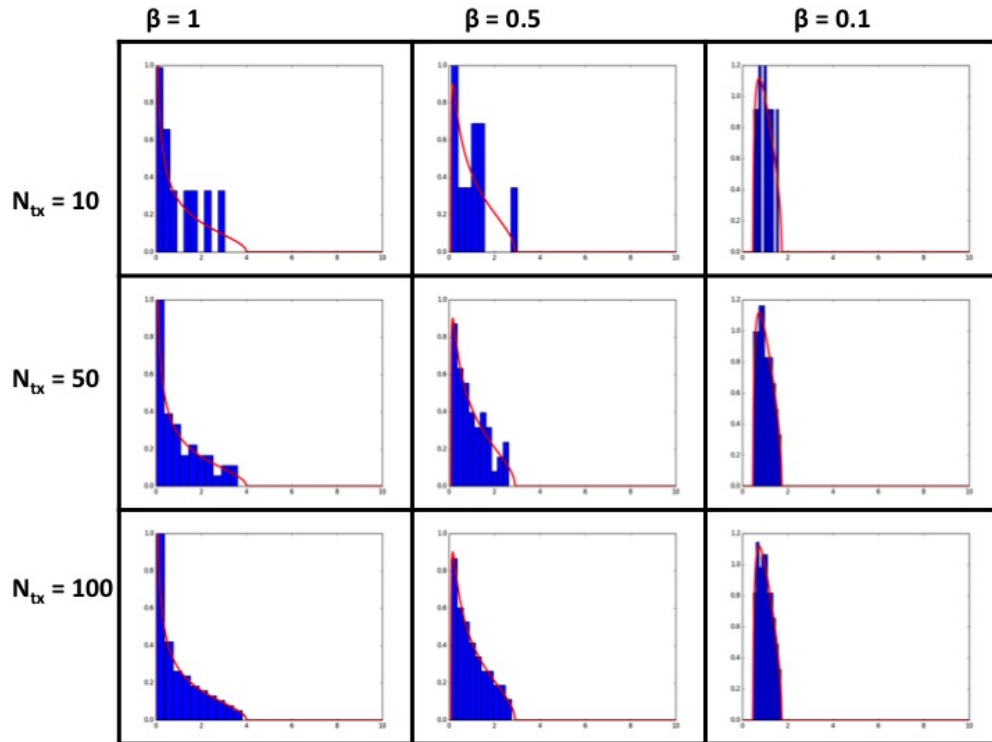


Figure 2: The distribution of diffraction gains under weak turbulence and the Marcenko-Pastur density for various  $\beta$ .

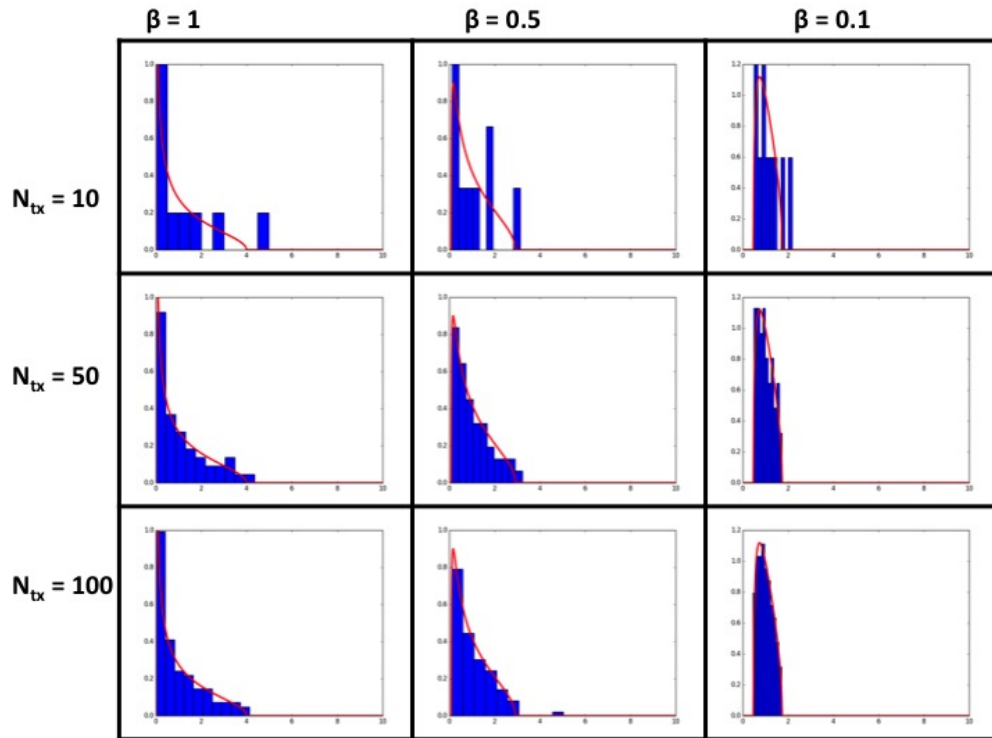


Figure 3: The distribution of diffraction gains under strong turbulence and the Marcenko-Pastur density for various  $\beta$ .

## Bit Error Rate

The maximum singular value is important for computing the lower limit on the bit error rate for this channel. For this computation, we assume that we have perfect knowledge of the channel, i.e. instantaneous feedback. Therefore, at any given time, we know exactly the transfer matrix  $\mathbf{H}$  and we can compute  $\mathbf{U}\mathbf{V}^\dagger$ . We further assume that we are communicating via binary phase shift keying, such that we have two signal vectors  $\vec{x}$  and  $-\vec{x}$ . In order to minimize the bit error rate of transmission, we choose  $\vec{x} = \vec{v}_{\max}$  such that we maximize the diffraction gain of the input signal across the channel.

In the absence of the additive white Gaussian noise  $\vec{w}$ , the detection statistic  $\phi = \text{Re}\{\vec{u}_{\max}^\dagger \vec{y}\}$  is sufficient to achieve perfect detection. Including noise,  $\phi|\vec{x}$  is a normally distributed random variable with mean  $\sqrt{\text{SNR}}(\mathbf{H}\vec{v}_{\max})$  and variance 1. If the two bits are equiprobable, the probability of error can be described by the tail of this distribution, and the probability of error given  $\mathbf{H}$  is  $Q\left(\sqrt{2\text{SNR}\gamma_{\max}^2}\right)$ .

As  $n_{tx}, n_{rx} \rightarrow \infty$ , from Marcenko-Pastur we know that  $\gamma_{\max}^2$  converges to  $(1 + \sqrt{\beta})^2$ . The Tracy-Widom law tells us about the fluctuation of  $\gamma_{\max}^2$  around that value. Thus the Tracy-Widom law gives us insight into the instantaneous bit error rate, and the Marcenko-Pastur density gives us insight into the average bit error rate (in the case of instantaneous feedback).

Figure 4 shows the empirical distribution of the bit error rate for varying  $n_{tx}$  with  $\beta = 1$ . We sample the transfer matrix distribution for 100 trials of 1000 bits each. The variance of the distribution clearly decreases as  $n_{tx}$  grows. As  $n_{tx} \rightarrow \infty$ , this distribution can be represented as the Q-function of a scaled Tracy-Widom distribution, and we can use known characteristics of the Tracy-Widom distribution to describe the behavior of the bit error rate. We can use the CDF of the Tracy-Widom distribution to describe the outage probability of the channel, i.e. the probability that the instantaneous bit error rate is less than some fixed  $P$ .

The average bit error rate should converge to

$$Q\left(\sqrt{2\text{SNR}\left(1 + \sqrt{\beta}\right)^2}\right)$$

We plot the simulated average bit error rate in Figure 5 against this theoretical prediction. For  $n_{tx} = 100$ , the average bit error rate matches the prediction closely. This expression for the bit error rate provides a lower limit on the achievable bit error rate for a particular channel.

Thus we have used results from random matrix theory to bound the performance of the turbulent free-space optical communication channel.

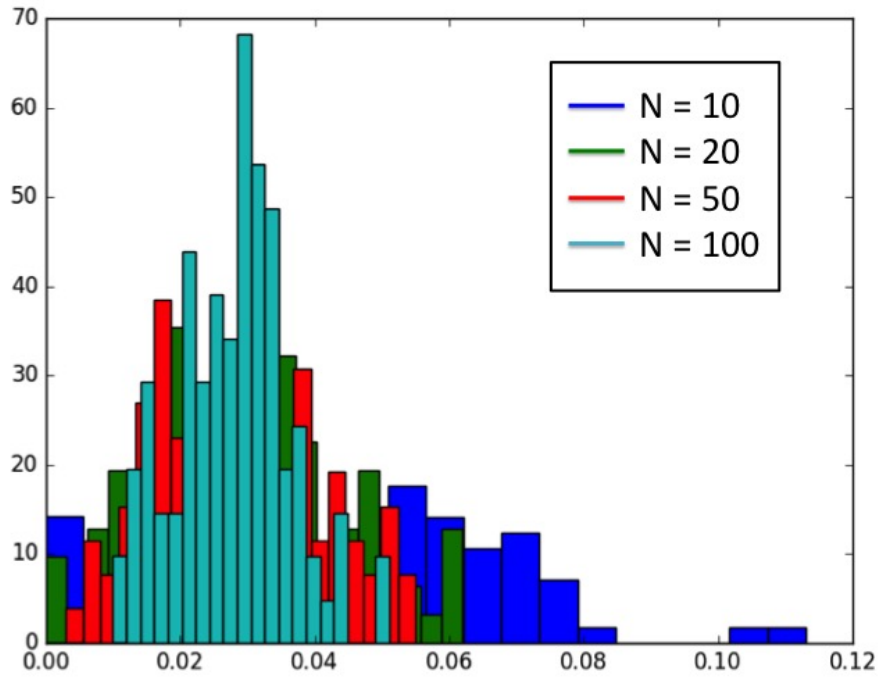


Figure 4: The empirical distribution of the bit error rate over one hundred trials, with  $\beta = 1$  and varying number of apertures. SNR = 0.5.

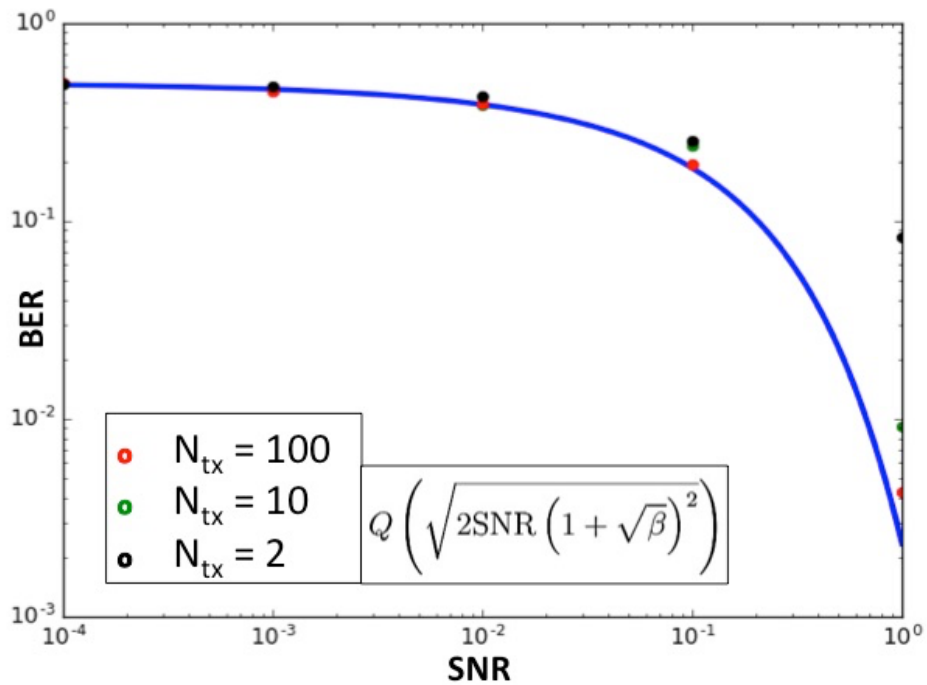


Figure 5: The average bit error rate of simulated 1000-bit transmissions with  $\beta = 1$  and varying number of apertures.

## Code

**using** PyPlot, ODE, Interact, Distributions;

### Simulate Channel Transfer Matrix

```
function generateH(N_rx,N_tx,L,C_n2)

    ##Log-amplitude fluctuations
    varX = minimum([0.124*k^(7/6)*C_n2*L^(11/6),0.5]);
    mX = -varX;
    Z = randn(N_rx,N_tx);
    X = e.^(Z*sqrt(varX) + mX);

    ##Log-phase fluctuations
    phi = rand(N_rx,N_tx) * 2 * pi;

    ##Channel Transfer Matrix
    H = X.*e.^(im*phi);

end
```

### Compute Marcenko-Pastur Distribution

```
function M_P(x,Beta)
    if x == 0
        f = 0;
    else
        num1 = maximum([0;(x-(1-sqrt(Beta))^2)]);
        num2 = maximum([0;((1+sqrt(Beta))^2-x)]);
        f = sqrt(num1*num2)./(2*pi*x*Beta);
    end
end
```

### Compare Simulated Diffraction Gain to Marcenko-Pastur Distribution

```
function compareDiffGain(N_rx,N_tx,L,C_n2)
    H = generateH(N_rx,N_tx,L,C_n2);
    A = H*H'/N_rx;
    gamma = eigvals(A);
    Beta = N_tx/N_rx;
    plt[:hist](gamma,normed=true);
    x = 0:.01:10
    f = zeros(1001);
    for i=1:1001
        f[i] = M_P(x[i],Beta);
    end
    plot(x,f,"r",linewidth=3);
    axis([0;10;0;1]);
    return gamma;
end
```

## Simulate Bit Transmission

### Compare Average Bit Error Rate to Asymptotic Theoretical Value

```
function AvgBER(bitstream, N_rx,N_tx,L,C_n2,SNR,trials)
    B = 0;
    for i=1:trials
        H = generateH(N_rx,N_tx,L,C_n2);
        F = svdfact(H/sqrt(N_rx));
        Vmax = F[:V][:,1];
        Umax = F[:U][:,1];
        seqLength = length(bitstream);
        suffStat = zeros(seqLength);
        for k = 1:seqLength
            w = randn(N_rx);
            y = sqrt(SNR/N_rx)*H*Vmax*bitstream[k] + w;
            suffStat[k] = real(Umax'*y)[1];
        end
        outstream = sign(suffStat);
        accuracy = sum(bitstream .== outstream)/seqLength;
        BER = 1-accuracy;
        B = B + BER;
    end
    B = B/trials;
    Q = 1 - cdf(Normal(),sqrt(2*SNR*(1+sqrt(N_tx/N_rx))^2));
    return B, Q;
end
```

### Compute Outage Probability

```
function OutageProb(bitstream, N_rx,N_tx,L,C_n2,SNR,trials)
    B = zeros(trials);
    for i=1:trials
        H = generateH(N_rx,N_tx,L,C_n2);
        F = svdfact(H/sqrt(N_rx));
        Vmax = F[:V][:,1];
        Umax = F[:U][:,1];
        seqLength = length(bitstream);
        suffStat = zeros(seqLength);
        for k = 1:seqLength
            w = randn(N_rx);
            y = sqrt(SNR/N_rx)*H*Vmax*bitstream[k] + w;
            suffStat[k] = real(Umax'*y)[1];
        end
        outstream = sign(suffStat);
        accuracy = sum(bitstream .== outstream)/seqLength;
        BER = 1-accuracy;
        B[i] = BER;
    end
    Bcdf, Bbins = plt[:hist](B,20,cumulative=true,normed=true);
    return B, Bcdf, Bbins;
end
```

## References

- [1] A. L. Puryear, Vincent W. S. Chan, “Optical communication through the turbulent atmosphere with transmitter and receiver diversity, wavefront control, and coherent detection,” *Proceedings of SPIE*, Vol. 7464, 2009.
- [2] A.L. Puryear, “Optical Communication Through the Turbulent Atmosphere With Transmitter and Receiver Diversity, Wavefront Control, and Coherent Detection,” *Ph.D. Thesis*, Massachusetts Institute of Technology, Cambridge, Massachusetts, 2011.